Corrosion Science 209 (2022) 110680

Contents lists available at ScienceDirect

Corrosion Science

journal homepage: www.elsevier.com/locate/corsci

Dissociative adsorption of azoles on Cu(111) promoted by chemisorbed O and OH

Anton Kokalj *, Matjaž Dlouhy

Department of Physical and Organic Chemistry, Jožef Stefan Institute, Jamova 39, SI-1000 Ljubljana, Slovenia
Jožef Stefan International Postgraduate School, Jamova 39, SI-1000 Ljubljana, Slovenia

ARTICLE INFO

Keywords:
Density-functional-theory calculations
Dissociative chemisorption
Coadsorption
Corrosion inhibitors
Copper

ABSTRACT

Metal surfaces are usually either oxidized or at least covered with species such as O and OH under ambient conditions. We show by DFT calculations that chemisorbed O and OH species promote deprotonation of azole molecules on copper surfaces, as exemplified herein by imidazole, benzotriazole, and Cu(111). Deprotonation involves the N–H bond cleavage, although imidazole can also deprotonate via the C–H cleavage. Calculated deprotonation activation energies are considerably smaller for the cleavage of the N–H bond (0.01 eV for benzotriazole and about 0.1 eV for imidazole) than for the cleavage of the C–H bond (from 0.6 to 0.9 eV for imidazole), although the cleavage of C–H bond is thermodynamically preferred for imidazole. Deprotonation reaction energies do not depend strongly on the coverage of O and OH, and for coverages from 1/16 to 1/4 ML, reaction energies typically alter by about ±0.1 eV. The importance of molecular deprotonation upon adsorption is in higher stability of the resulting adsorption states, which increases the persistence of chemisorbed molecules. In particular, deprotonated benzotriazole molecules are by about 1 eV more stable on O/Cu(111) and OH/Cu(111) compared to an adsorbed intact molecule on bare Cu(111). In contrast, for imidazole, the magnitude of such stabilization is significantly weaker (from 0.3 to 0.7 eV).

1. Introduction

One way to mitigate corrosion is to use organic corrosion inhibitors, which are substances that effectively reduce the rate of corrosion of metals and alloys already when used in relatively low concentrations. It is generally accepted that inhibitors reduce corrosion by adsorbing to the surface, thus protecting it [1]. It is, therefore, not surprising that many computational studies, based on density-functional theory (DFT), addressed the adsorption of corrosion inhibitors. However, most of them considered bare metal surfaces (e.g., see the recent review [2]). Obot etal [3] criticized such calculations as naive because metal surfaces are probably never clean in real environments; even during active dissolution, they are likely covered with adsorbed species such as O, OH, H, and Cl. For this reason, we addressed in our previous publication [4] how such species (hereinafter labeled as $X_{(ads)}$) affect the non-dissociative adsorption of imidazole on copper surfaces, where imidazole was used as an archetypal toy model of azole[1] corrosion inhibitors. We showed that such species could affect the azole–surface interaction in three ways: (i) via modification of the surface work function, which affects the molecule–surface bonding. This effect depends linearly on the coverage of $X_{(ads)}$ and can either stabilize or destabilize the adsorbed azole molecule. (ii) Chemisorbed species, such as O and OH, can form stabilizing hydrogen bonds with adsorbed azole molecules; and (iii) chemisorbed O and Cl enhance the N–Cu bond between the nearby adsorbed imidazole and the surface. This effect decreases with decreasing coverage of $X_{(ads)}$ but does not vanish at zero coverage.

There is at least one further effect of how the $X_{(ads)}$ species affect the adsorption of azole molecules that was not considered in our previous publication [4] and is therefore considered herein. This effect is the aftermath of the effect (ii), i.e., once the hydrogen bond between either O or OH and nearby azole is formed, the adsorbed molecule can be further stabilized by deprotonation that involves a proton shift from a molecule to chemisorbed O or OH. To this end, we consider dissociative adsorption of imidazole and benzotriazole molecules—their skeletal structures are shown in Fig. 1—on Cu(111) covered with either $O_{(ads)}$ or $OH_{(ads)}$. While imidazole is seldom used as a corrosion inhibitor [5], it can be seen as an archetypal model of imidazole-based corrosion inhibitors. In contrast, benzotriazole is an outstanding and widely used corrosion inhibitor for copper [6]. Although adsorption of imidazole

* Corresponding author at: Department of Physical and Organic Chemistry, Jožef Stefan Institute, Jamova 39, SI-1000 Ljubljana, Slovenia.
E-mail address: tone.kokalj@ijs.si (A. Kokalj).
URL: http://www.ijs.si/ijsw/K3-en/Kokalj (A. Kokalj).

[1] Azoles are five-membered aromatic molecules containing one nitrogen atom and at least one other heteroatom (N, O, or S).

https://doi.org/10.1016/j.corsci.2022.110680
Received 16 May 2022; Received in revised form 12 September 2022; Accepted 18 September 2022
Available online 24 September 2022

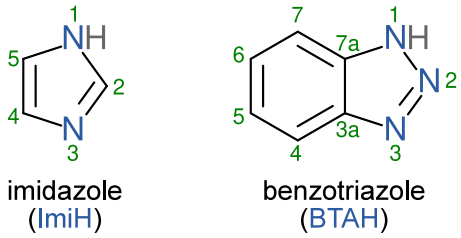

Fig. 1. Skeletal structures of imidazole and benzotriazole molecules. The numbering of atoms and molecular shorthand labels are also indicated.

and benzotriazole on copper surfaces have been widely studied by DFT methods [7–20], the issues considered herein have not yet been thoroughly addressed. The choice of these two molecules was motivated by the following consideration. Deprotonation of benzotriazole involves the cleavage of the N–H bond [21], whereas deprotonation of adsorbed imidazole can also involve the cleavage of the C–H bond [22]. These two molecules thus cover the two qualitatively different cases: deprotonation of an azole molecule either at a heteroatom or at a C atom.

A stabilization of adsorbed inhibitor molecules by $O_{(ads)}$ and $OH_{(ads)}$ is relevant for corrosion inhibition because, under the premise that inhibitors reduce corrosion by adsorbing to the surface, they should adsorb strong enough, or else they would quickly desorb. We thus also estimate the residence times of adsorbed molecules on Cu(111) and show that chemisorbed O and OH can stabilize adsorbed benzotriazole to such an extent that its adsorption can be considered irreversible at room temperature.

2. Technical details

2.1. Computational method

DFT calculations were performed with Quantum ESPRESSO [23,24] using the PBE+D" method [25] that consists of the Perdew–Burke–Ernzerhof (PBE) exchange–correlation functional [26] and a reparametrized[2] D2 empirical dispersion correction of Grimme [27]. Kohn–Sham orbitals were described with a plane wave basis set using a kinetic energy cutoff of 30 Ry (240 Ry for the charge density). Core electrons were represented by ultrasoft-pseudo potentials [28,29]. The PWTK scripting environment [30] was used to automate computational workflows.

Cu(111) was modeled by a periodic multi-slab model consisting of four (111) layers. The bottom layer was constrained to the bulk positions compatible with the calculated equilibrium Cu bulk lattice parameter of 3.65 Å. Adsorbates were adsorbed on the top side of the slab, and a dipole correction of Bengtsson [31] was applied. Brillouin-zone integrations were performed with the special point technique [32] using the Methfessel–Paxton smearing [33] of 0.03 Ry and a shifted $4 \times 4 \times 1$ k-point mesh for the (4×4)–Cu(111) supercell.

Dissociation activation energies were calculated with the climbing image nudged elastic band (CI-NEB) method [34,35], where a reaction pathway is modeled as a minimum energy path (MEP) between a reactant (initial state, IS) and a product (final state, FS). A transition state (TS) is the maximum energy configuration on the MEP, and the activation energy (E^*) is calculated as the difference between the TS and IS energies:

$$E^* = E_{TS} - E_{IS}. \tag{1}$$

[2] The C_6 parameter of Cu was reparametrized from the original value of 375 Ry/Bohr^6 to the value of 140 Ry/Bohr^6 [25] as to reduce the molecule–surface overbinding of the original PBE+D2 method.

The threshold for the magnitude of the atomic force components in CI-NEB calculations was set to 50 meV/Å.

Calculations presented herein correspond to *in-vacuo* calculations unless explicitly stated otherwise. However, some calculations were also performed with an aqueous solvent described implicitly by the soft-sphere-continuum-solvation method [36] as implemented in the `Environ` plugin [37] for Quantum ESPRESSO. Due to convergence problems, we could only perform single-point SCF calculations on the structures relaxed in a vacuum.

Molecular graphics were produced by the `xcrysden` graphical package [38]. XY plots were plotted with the `Gnuplot` program [39], and post-processing of figures was done in `Inkscape` [40].

2.2. Definitions of labels

MolH is used as a generic label to indicate a molecule, and the ImiH and BTAH labels are used as shortcuts for the imidazole and benzotriazole molecules, respectively. X is used as a generic label to designate the O and OH species. The Cu(111) surface, covered with X species, is labeled as X/Cu(111), whereas a molecule adsorbed on X/Cu(111) is labeled as either MolH @ X/Cu(111) or MolH + X @ Cu(111), depending on the focus.

Mol (note that H is omitted) is used as a generic label to indicate a deprotonated molecule, whereas the Imi and BTA labels denote deprotonated imidazole and benzotriazole molecules, respectively.

2.3. Surface coverage

The surface coverage is expressed in monolayer (ML) units, defined as the inverse of the number of surface Cu atoms per adsorbate. Herein, we consider only 1/16 ML coverage of MolH, corresponding to one molecule per (4×4)–Cu(111) supercell. For $X_{(ads)}$, coverages from 1/16 to 4/16 ML are considered (i.e., the number of $X_{(ads)}$ species per (4×4)–Cu(111) supercell ranges from one to four). For this reason, the stated coverage always corresponds to the coverage of $X_{(ads)}$ unless explicitly stated otherwise.

2.4. Energy equations

The molecular adsorption binding energy (E_b) is calculated as:

$$E_b = E_{MolH/Cu(111)} - (E_{Cu(111)} + E_{MolH}), \tag{2}$$

where $E_{MolH/Cu(111)}$ is the total energy of a molecule/Cu(111) system, $E_{Cu(111)}$ is the total energy of a bare Cu(111) slab, and E_{MolH} is the total energy of an isolated molecule.

To address how $X_{(ads)}$ species affect the molecular non-dissociative adsorption binding energy, we defined ΔE_b as:

$$\Delta E_b = E'_b - E_b, \tag{3}$$

where E_b is the molecular binding energy on bare Cu(111), calculated with Eq. (2), whereas E'_b is the molecular binding energy on X/Cu(111), calculated as:

$$E'_b = E_{MolH/X/Cu(111)} - (E_{X/Cu(111)} + E_{MolH}) \tag{4}$$

where $E_{MolH/X/Cu(111)}$ and $E_{X/Cu(111)}$ are total energies of the MolH @ X/Cu(111) co-adsorption system and X/Cu(111), respectively.

A change of energy as a system goes from one state (say, state A) to another state (state B) is denoted by a generic label ΔE and is calculated as:

$$\Delta E = E_B - E_A, \tag{5}$$

where E_A and E_B are total energies of states A and B, respectively.

Adsorption energies are calculated with respect to an isolated MolH molecule in a vacuum. Depending on the substrate, adsorption energy of non-dissociative adsorption is equivalent to either E'_b or E_b, i.e.:

$$E_{ads} = E_{MolH/surf} - (E_{surf} + E_{MolH}), \tag{6}$$

where "surf" stands for either X/Cu(111) or bare Cu(111). For deprotonated molecules, adsorption energy is calculated as:

$$E_{ads}^{diss} = E_{(Mol+H)/surf} - (E_{surf} + E_{MolH}), \quad (7)$$

where $E_{(Mol+H)/surf}$ is the total energy of an adsorption system with H and deprotonated Mol coadsorbed on the surface; the superscript "diss" in E_{ads}^{diss} indicates "dissociative" adsorption.

3. Results and discussion

$X_{(ads)}$ species do not only affect the non-dissociative adsorption of azole molecules, as demonstrated in our previous publication [4], but in some cases also promote a bond-breaking, such as molecular deprotonation, leading to further stabilization of adsorbed molecules [22,41,42]. Here we consider the following two molecular deprotonation reactions:

$$MolH_{(ads)} + O_{(ads)} \rightarrow Mol_{(ads)} + OH_{(ads)} \quad (8)$$

and

$$MolH_{(ads)} + OH_{(ads)} \rightarrow Mol_{(ads)} + H_2O_{(ads)}. \quad (9)$$

Note that $O_{(ads)}$ and $OH_{(ads)}$ reactants are consumed in these two reactions. For this reason, from now on, the coverage of $O_{(ads)}$ and $OH_{(ads)}$ always corresponds to the coverage of reactant $O_{(ads)}$ and $OH_{(ads)}$. The corresponding deprotonation reaction energies ($\Delta E_{deproto}$) are calculated as:

$$\Delta E_{deproto} = E_{FS} - E_{IS}, \quad (10)$$

where E_{IS} and E_{FS} stand for total energies of initial (reactants) and final (products) states in reaction (8) or (9).

The total stabilization of molecular adsorption (ΔE_{stab}^{tot}) induced by $X_{(ads)}$ is given by the sum of ΔE_b and $\Delta E_{deproto}$, i.e.:

$$\Delta E_{stab}^{tot} = \Delta E_b + \Delta E_{deproto}, \quad (11)$$

where ΔE_b corresponds to the $X_{(ads)}$ induced enhancement of the MolH adsorption bonding and $\Delta E_{deproto}$ to the additional stabilization due to a deprotonation reaction.

3.1. Dissociative adsorption on bare Cu(111)

To better appreciate the role of $O_{(ads)}$ and $OH_{(ads)}$ in molecular deprotonation reactions on copper surfaces, let us first consider dissociation reactions involving the Mol–H cleavage on bare Cu(111), i.e.:

$$MolH_{(ads)} \rightarrow Mol_{(ads)} + H_{(ads)}. \quad (12)$$

However, on bare Cu(111) this reaction would be more appropriately referred to as H-abstraction rather than deprotonation because H adsorbed to bare Cu(111) is negatively charged (its Bader charge is −0.32 [4]), hence it is hydride- and not proton-like. Also on Cu_2O surfaces, H is negatively charged if adsorbed to Cu ions, but it is proton-like if adsorbed to O ions [42].

Fig. 2 presents the PBE+D" calculated H-abstraction reaction energies for BTAH and ImiH adsorbed on bare Cu(111) along with the corresponding initial- and final-state structures (these calculations were performed with one molecule per (4×4)–Cu(111) supercell). H-abstraction of BTAH involves the N1–H bond cleavage, and the reaction energy is slightly exothermic, $\Delta E = -0.18$ eV at 1/16 ML,[3] whereas the activation barrier was calculated in our older study [21] to be about

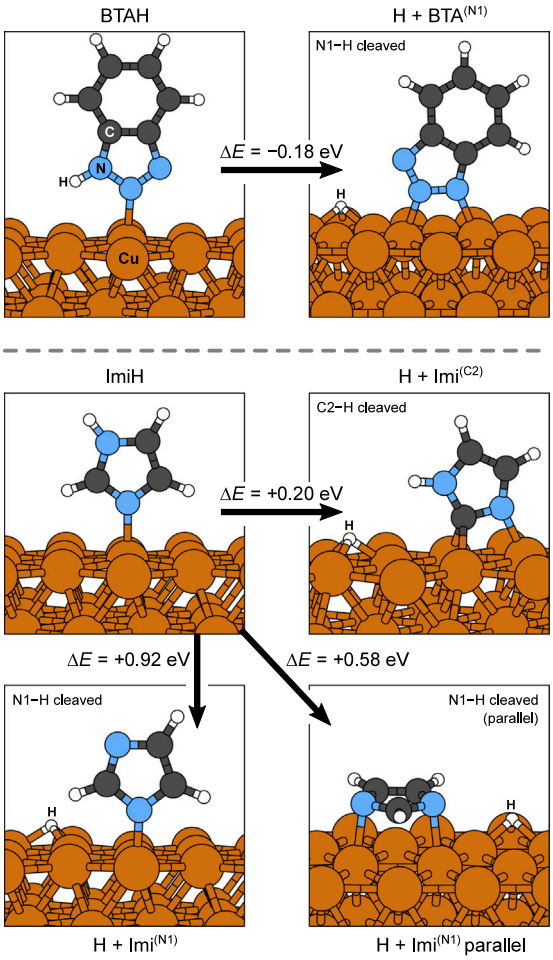

Fig. 2. H-abstractions from BTAH (top) and ImiH (middle and bottom) adsorbed on bare (4 × 4)–Cu(111). The PBE+D"-calculated reaction energies (ΔE) are given. The superscript in the $BTA^{(N1)}$ label indicates that H-abstraction involved the cleavage of the N1–H bond and analogously for the $Imi^{(N1)}$ and $Imi^{(C2)}$ labels. Note that for imidazole, the cleavage of the C2–H bond is superior to the N1–H bond cleavage.

1 eV. In contrast to BTAH, the N1–H bond cleavage of imidazole was calculated to be significantly endothermic, both on Cu(111) [43] and Cu_2O surfaces [42]. According to the current PBE+D" results (Fig. 2), the reaction energy for the N1–H bond cleavage of adsorbed ImiH is +0.92 eV for perpendicular and +0.58 eV for parallel adsorbed Imi. The inferiority of the imidazole N1–H cleavage can be attributed to its molecular geometry because it has the two N atoms on opposite sides of the molecule and a "deprotonated" molecule needs to form at least two strong molecule–surface bonds to compensate for the broken N–H bond [22,42–44]. The other, more stable alternative is parallel adsorption of imidazole, where both N atoms bond to the surface, but these two N–Cu bonds are strained. Hence even in this case, the N1–H cleavage of imidazole is considerably inferior to that of BTAH.

Although it seems chemically intuitive that deprotonation of imidazole should proceed via the cleavage of the N1–H bond, we found in the previous publication [22] that on Cu_2O surfaces (and also on Fe(100) [45]), the cleavage of the C2–H bond is instead thermodynamically preferred. Current results (Fig. 2) also show this to be the case on bare Cu(111), where the reaction energy of +0.2 eV is substantially smaller (less endothermic) than for the cleavage of the N1–H bond. In the following subsection, we show that the C2–H bond cleavage of imidazole is thermodynamically preferred over the N1–H bond cleavage also on O/Cu(111) and OH/Cu(111).

[3] This value of ΔE is more exothermic than the value of about +0.1 eV reported in our older study [21]. The reason is that in the older study, the value corresponds to BTA and H co-adsorbed to adjacent nearest-neighbor sites where they experience some lateral repulsion.

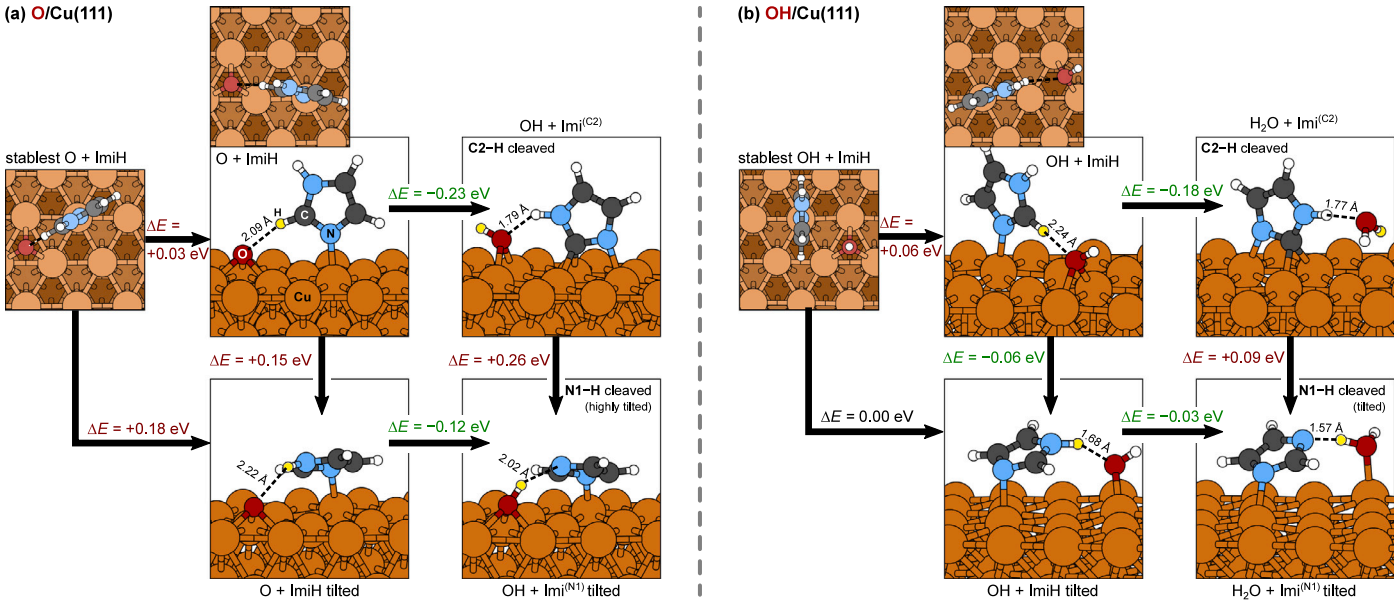

Fig. 3. C2–H and N1–H bond cleavages of ImiH on (4 × 4)–X/Cu(111), X = O (left) and OH (right). The smaller top-view snapshots on the left in (a,b) show the most stable identified ImiH adsorption structures (labeled as "stablest"), whereas the perspective side-view snapshots in (a,b) show the structures used in the NEB bond-cleavage calculations. The relative stability among the shown structures is indicated by ΔE. The C2–H bond cleavage is preferred over the N1–H one by 0.26 and 0.09 eV on O/Cu(111) and OH/Cu(111), respectively. The proton (H atom) that reacts is highlighted in yellow. (For interpretation of the references to color in this figure legend, the reader is referred to the web version of this article.)

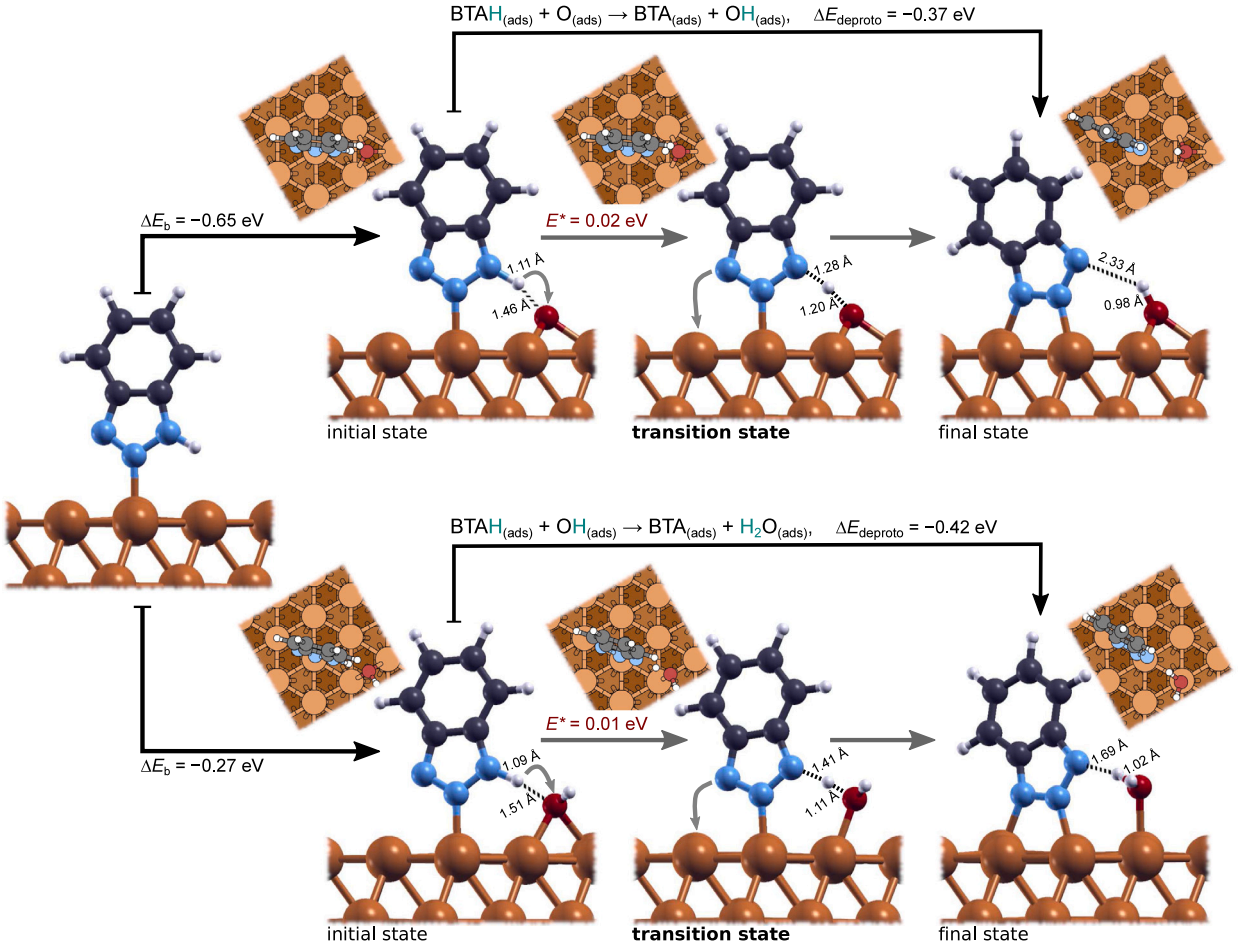

Fig. 4. Deprotonation of BTAH on Cu(111) induced by $O_{(ads)}$ (top row) and $OH_{(ads)}$ (bottom row) at 1/16 ML. From left to right: BTAH adsorbed on Cu(111), BTAH adsorbed near $O_{(ads)}$ and $OH_{(ads)}$ thereon (labeled as the initial state), transition state of deprotonation, and deprotonated BTA (final state). PBE+D" calculated characteristic energies and bond lengths are also stated, i.e., $\Delta E_b = X_{(ads)}$ induced stabilization of BTAH; $\Delta E_{deproto}$ = deprotonation reaction energy; E^* = deprotonation activation energy.

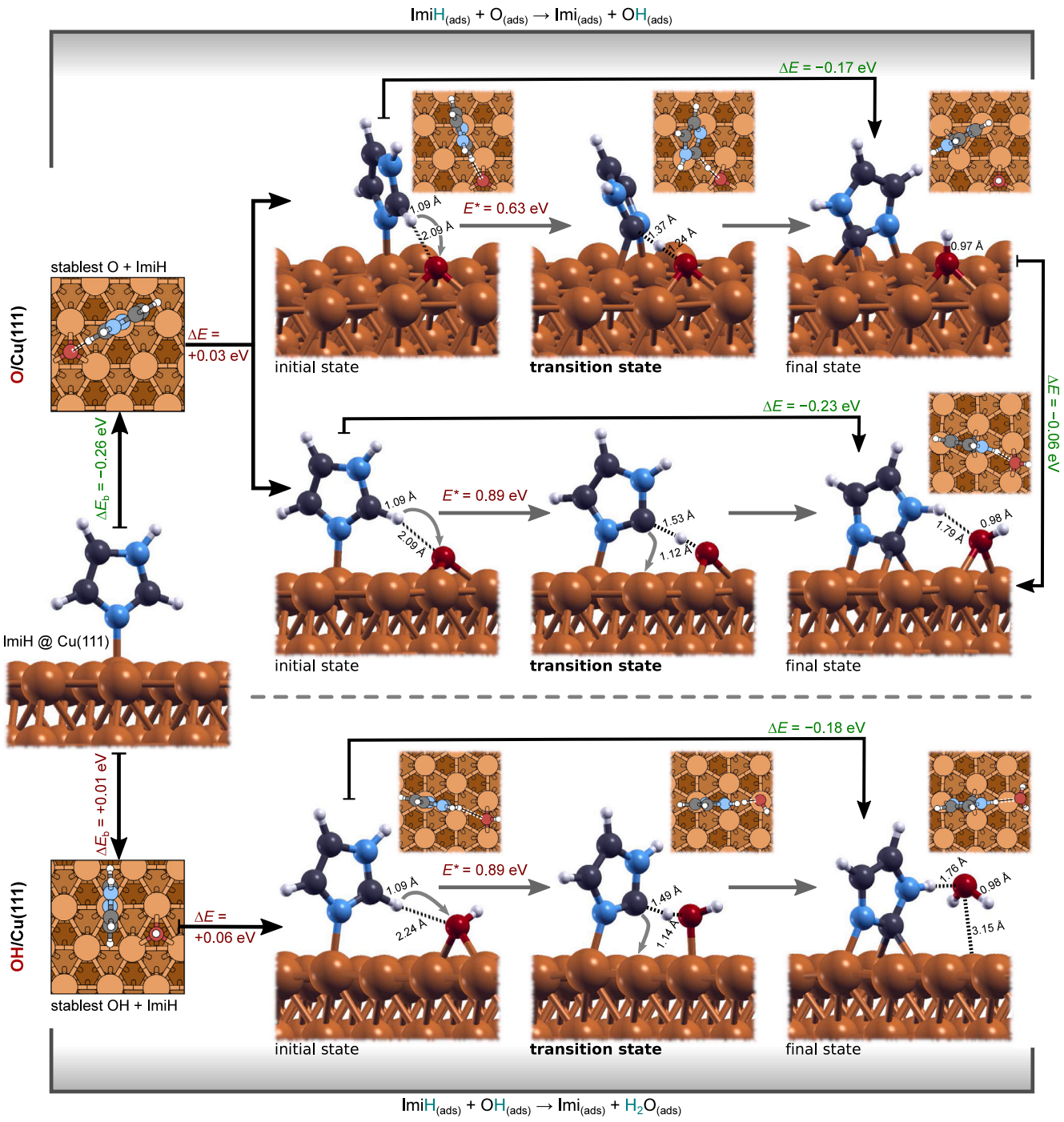

Fig. 5. Similar to Fig. 4, but for the C2–H bond cleavage of imidazole. On the far left, ImiH on Cu(111) and the most stable identified ImiH structures on O/Cu(111) [top] and OH/Cu(111) [bottom] are shown, followed by (from left to right) the reaction initial-, transition-, and final-state structures. Two reaction paths are considered for the $O_{(ads)}$ induced deprotonation of ImiH. The upper reaction path results in OH adsorbed onto an fcc-hollow site, whereas in the lower reaction path, the final state consists of OH adsorbed to a bridge site and an N1H···O hydrogen bond between deprotonated imidazole and OH. The latter final state is marginally more stable than the former, by 0.06 eV, but the former reaction path displays a significantly smaller deprotonation barrier (0.63 eV) compared to the latter one (0.89 eV).

3.2. N1–H vs. C2–H bond cleavage of imidazole on X/Cu(111)

Fig. 3 presents the PBE+D" calculated reaction energies for the N1–H and C2–H bond-cleavage reactions on (4 × 4)–O/Cu(111) and (4×4)–OH/Cu(111). Here, the reaction energies are considerably more favorable than on bare Cu(111). In contrast to Cu(111), C2–H bond-cleavage reaction is exothermic on both surfaces, whereas the N1–H cleavage is marginally exothermic only on OH/Cu(111). The C2–H bond cleavage is thermodynamically preferred over the N1–H cleavage by 0.26 and 0.09 eV on O/Cu(111) and OH/Cu(111), respectively.

We should comment that the most stable identified adsorption structures of ImiH on O/Cu(111) and OH/Cu(111)—shown on the far left in Figs. 3a and 3b—are usually not directly used in the NEB bond-cleavage calculations. In such cases, the reaction consists of two elementary steps: rearrangement of ImiH to an adequately oriented structure followed by the actual bond-cleavage step.[4] On (4 × 4)–O/Cu(111), the

[4] With respect to the adsorption site designation used in our previous publication [4], the most stable ImiH structures are adsorbed onto the blue site

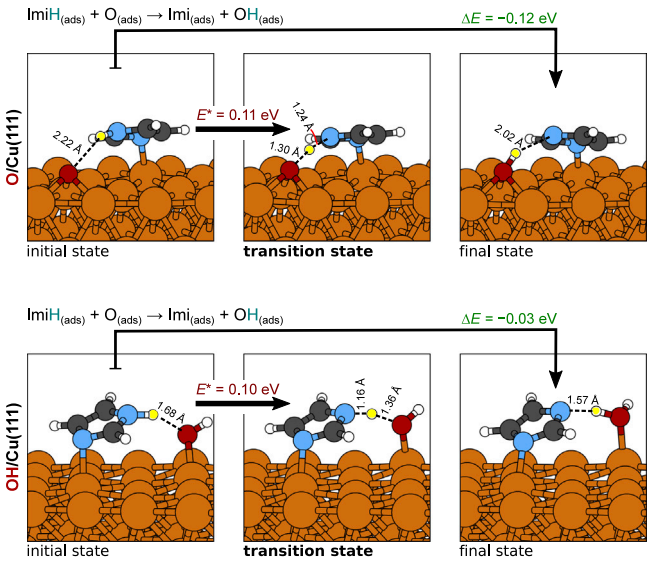

Fig. 6. The N1–H bond-cleavage reactions of imidazole on O/Cu(111) [top row] and OH/Cu(111) [bottom row]. PBE+D" calculated activation energies, reaction energies, and H-bond lengths are also stated (note that the shown initial-state ImiH structure on O/Cu(111) is by 0.18 eV less stable than the stablest ImiH structure, see Fig. 3). The proton (H atom) that reacts is highlighted in yellow. (For interpretation of the references to color in this figure legend, the reader is referred to the web version of this article.)

most stable identified ImiH structure is by 0.03 eV and 0.18 eV more stable than those used for the C2–H and N1–H cleavage reactions, respectively, whereas on (4 × 4)–OH/Cu(111), these differences are 0.06 eV and 0.00 eV, respectively. Hence, on OH/Cu(111), the tilted ImiH structure used for the N1–H cleavage reaction is as stable as the structure labeled the "stablest" in Fig. 3b. The high stability of the tilted structure is due to the H-bond with the nearby OH group, i.e., the N1H···O bond.

For the sake of completeness, both the C2–H and N1–H bond-cleavage reactions of imidazole are considered in more detail in the following subsection.

3.3. Deprotonations on X/Cu(111) at low 1/16 ML coverage

Calculated activation and reaction energies along with the initial, transition, and final-state structures for deprotonation reactions (8) and (9) on X/Cu(111) are shown in Fig. 4 for BTAH and in Figs. 5 (C2–H bond cleavage) and 6 (N1–H bond cleavage) for ImiH. The reactions were modeled at a molecular coverage of 1/16 ML using the (4 × 4)–MolH @ X/Cu(111) systems, i.e., the (4 × 4) supercell contained one X species and one MolH molecule.

3.3.1. N1–H bond cleavage of benzotriazole

Fig. 4 reveals that at 1/16 ML coverage, $O_{(ads)}$ and $OH_{(ads)}$ stabilize an intact adsorbed BTAH by 0.65 and 0.27 eV, respectively, which can be attributed to the three effects explained in the introduction. $BTAH_{(ads)}$ forms a strong NH···O hydrogen bond with $O_{(ads)}$ and $OH_{(ads)}$. The strength of this hydrogen bond is estimated to be about 0.3 ± 0.1 eV [46]. Therefore, the formed hydrogen bond almost entirely explains the $OH_{(ads)}$ induced stabilization of adsorbed BTAH. In contrast, $O_{(ads)}$ also enhances the N–Cu bond between the nearby adsorbed azole and the surface [4], which is why the $O_{(ads)}$ induced stabilization of intact adsorbed BTAH ($\Delta E_b = -0.65$ eV) is much stronger than the one induced by $OH_{(ads)}$ ($\Delta E_b = -0.27$ eV).

Adsorbed BTAH can further stabilize by about 0.4 eV by proton transfer from its N1 atom to either $O_{(ads)}$ or $OH_{(ads)}$. The calculated reaction energies of deprotonation reactions (8) and (9) at 1/16 ML are −0.37 and −0.42 eV, respectively. The results of Fig. 4 reveal that deprotonation of $BTAH_{(ads)}$ is not only thermodynamically favorable but also kinetically fast because the calculated activation energies are exceedingly small, being only 0.02 and 0.01 eV for reactions (8) and (9), respectively. These results are consistent with experimental studies that reported deprotonation of pyrazole [47] and triazole [48] on O/Cu(100) at low temperatures. The results are also compatible with the previous computational study [42] that reported exceedingly small or even vanishing activation energies for deprotonation of triazole and tetrazole on Cu_2O surfaces near oxygen vacancies (the role of oxygen vacancy is to allow deprotonated azole to form several N–Cu bonds). $O_{(ads)}$ and $OH_{(ads)}$ thus promote deprotonation of BTAH both thermodynamically and kinetically (for comparison, on clean Cu(111), the reaction energy is −0.18 eV (Fig. 2) and activation energy is about 1 eV [21]).

The total stabilization (ΔE^{tot}_{stab}) of adsorbed benzotriazole induced by $O_{(ads)}$ and $OH_{(ads)}$ at 1/16 ML is −1.02 and −0.69 eV, respectively (cf. Fig. 4). Although these values depend on the $X_{(ads)}$ coverage, as shown in the next subsection, they are sizable enough to conclude that both $O_{(ads)}$ and $OH_{(ads)}$ significantly stabilize adsorbed benzotriazole and induce its deprotonation, resulting in $BTA_{(ads)}$ on the copper surface.

3.3.2. C2–H bond cleavage of imidazole

Fig. 5 reveals that the calculated activation energies for the C2–H bond cleavage of imidazole are sizable (from 0.6 to 0.9 eV), and the corresponding reaction energies are less exothermic ($\Delta E_{deproto} \gtrsim -0.2$ eV) than for benzotriazole ($\Delta E_{deproto} \approx -0.4$ eV). Furthermore, $ImiH_{(ads)}$ is stabilized considerably less than $BTAH_{(ads)}$ by $O_{(ads)}$ and $OH_{(ads)}$ because the formed CH···O hydrogen bond between imidazole and $X_{(ads)}$ is considerably weaker than the NH···O hydrogen bond [46] between $BTAH_{(ads)}$ and $X_{(ads)}$. These aspects contribute to the outcome that $O_{(ads)}$ and $OH_{(ads)}$ stabilize imidazole considerably less than benzotriazole. In particular at 1/16 ML coverage of $X_{(ads)}$, the total stabilization (ΔE^{tot}_{stab}) of adsorbed imidazole induced by $O_{(ads)}$ and $OH_{(ads)}$ is −0.46 and −0.11 eV, respectively, whereas the corresponding values for benzotriazole are −1.02 and −0.69 eV. All these values can be deduced from Figs. 4 and 5.

For the C2–H bond-cleavage reaction on OH/Cu(111), two different reaction paths are presented in Fig. 5. They both involve the same initial state. The upper shown reaction path results in the final state with OH adsorbed into an fcc-hollow site (OH_{fcc}). In contrast, the lower shown reaction path results in OH adsorbed to a bridge site (OH_{br}) that forms an O···HN1 hydrogen bond with deprotonated imidazole. Although the final state with OH_{fcc} (upper reaction path) is marginally less stable (by 0.06 eV) than the final state with OH_{br} (lower reaction path), its deprotonation activation barrier of 0.63 eV is significantly lower than the activation energy of 0.89 eV for the reaction path leading to OH_{br}. As for the second imidazole deprotonation reaction, $ImiH_{(ads)} + OH_{(ads)} \rightarrow Imi_{(ads)} + H_2O_{(ads)}$, the calculated activation energy is 0.89 eV. Although the deprotonation barriers of 0.63 and 0.89 eV are sizable, they can be overcome at room temperature.[5] These two activation energies are smaller than the barrier of 1.1 eV reported

and those used herein for the C2–H bond-cleavage reaction onto the yellow site.

[5] A typical time scale (τ) of an elementary reaction event can be estimated from the inverted Arrhenius equation, $\tau = \nu^{-1} \exp(E^*/kT)$, where ν is the frequency prefactor and k is the Boltzmann constant. According to transition state theory, a typical value of ν is 10^{13} s^{-1}. At room temperature, this value of ν gives τ of about 4 ms and 100 s for reactions with E^* of 0.63 and 0.89 eV, respectively.

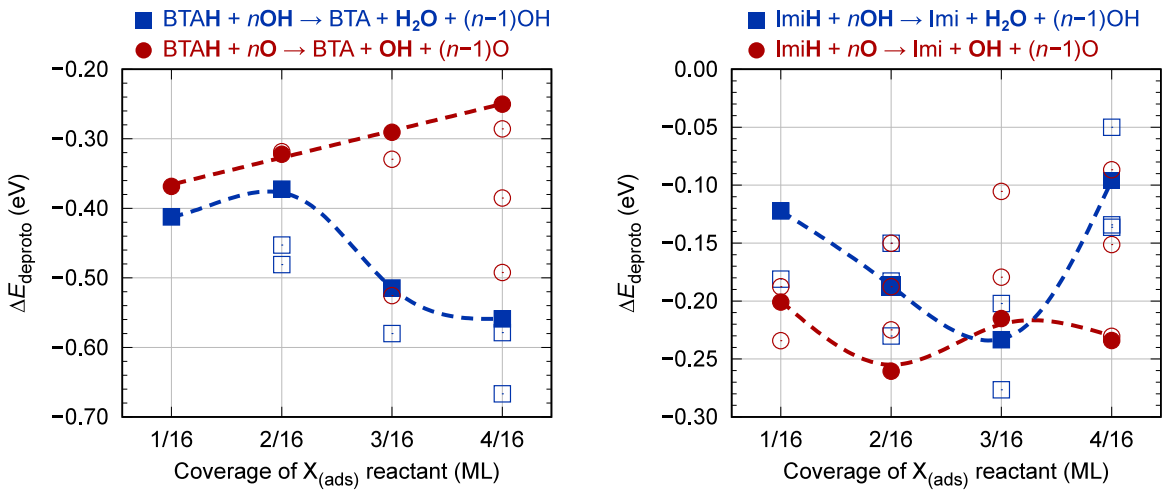

Fig. 7. Dependence of the BTAH (left) and ImiH (right) deprotonation reaction energies ($\Delta E_{\text{deproto}}$) on the coverage of $X_{(ads)}$ reactant. Beware of the different energy scales for BTAH and ImiH. Blue squares correspond to reactions with $OH_{(ads)}$ and red circles to reactions with $O_{(ads)}$. Curves are drawn to guide the eye. Different lateral configurations of adsorbates were considered, and the solid data points refer to the most stable identified reactant and product configurations at each coverage. In contrast, open points correspond to other less stable reactant and product configurations. (For interpretation of the references to color in this figure legend, the reader is referred to the web version of this article.)

for the C2–H bond cleavage of imidazole on $Cu_2O(111)$ near oxygen vacancy [22]. Sizable activation energies for the cleavage of the C–H bond are compatible with the experimental study [47] that reported the C–H bond cleavage of pyrazole on O/Cu(100) at elevated temperatures.

3.3.3. N1–H bond cleavage of imidazole

Although the N1–H bond cleavage of adsorbed imidazole is thermodynamically inferior to the C2–H bond cleavage (see Fig. 3), the calculations reveal that, kinetically, the N1–H bond cleavage is much easier with the activation energies of only about 0.1 eV on both O/Cu(111) and OH/Cu(111) (Fig. 6). It is worth noting from Fig. 6 that during the N1–H bond cleavage, the position of the imidazole molecule is relatively intact; it is only the proton that shifts from N1 to $O_{(ads)}$ or $OH_{(ads)}$.

With respect to the ImiH initial-state structures of Fig. 6, the N1–H bond-cleavage reactions are slightly exothermic on both surfaces. However, on O/Cu(111), the shown tilted ImiH initial-state structure is by 0.18 eV less stable than the stablest ImiH structure (see Fig. 3). In contrast, on OH/Cu(111) the tilted ImiH initial-state structure is as stable as the stablest perpendicular ImiH structure. Hence, with respect to the most stable ImiH structure, the N1–H bond cleavage is endothermic by 0.06 eV on O/Cu(111) and exothermic by 0.03 eV on OH/Cu(111).

3.4. Role of the $X_{(ads)}$ coverage

The above results refer to the $X_{(ads)}$ coverage of 1/16 ML, corresponding to the (4 × 4)–Cu(111) supercell containing one X species and one MolH molecule. To shed some light on how the coverage of $X_{(ads)}$ affects the deprotonation reaction energies, we considered the $X_{(ads)}$ coverages from 1/16 to 1/4 ML. To this end, calculations were performed with the (4 × 4)–Cu(111) supercell containing one MolH molecule and n X species with n ranging from 1 to 4. The corresponding deprotonation reactions can be written as:

$$\text{MolH}_{(ads)} + n\text{O}_{(ads)} \rightarrow \text{Mol}_{(ads)} + \text{OH}_{(ads)} + (n-1)\text{O}_{(ads)} \quad (13)$$

and

$$\text{MolH}_{(ads)} + n\text{OH}_{(ads)} \rightarrow \text{Mol}_{(ads)} + \text{H}_2\text{O}_{(ads)} + (n-1)\text{OH}_{(ads)}. \quad (14)$$

To make results more reliable, we performed a configurational search and calculated 98 different lateral configurations (their snapshots are shown in Figs. S1–S8 in the Supplementary material). For imidazole, only the thermodynamically favored C2–H bond cleavage was considered. The corresponding PBE+D" calculated $\Delta E_{\text{deproto}}$ results are shown in Fig. 7. The solid points refer to reactions involving the most stable identified reactant and product configurations at each $X_{(ads)}$ coverage (the respective snapshots are shown in Figs. S9–S12 in the Supplementary material). In contrast, open points correspond to other less stable reactant and product configurations.

Fig. 7 shows that all calculated deprotonation reaction energies are exothermic and do not show a strong dependence on the $X_{(ads)}$ coverage. Referring to the most stable configurations (solid points), the largest difference between $\Delta E_{\text{deproto}}$ at low and high $X_{(ads)}$ coverage appears for BTAH on OH-covered surface, where the value at 4/16 ML is more exothermic by 0.15 eV compared to low 1/16 ML coverage. The trends can be summarized as follows (referring again to the most stable points):

1. The $\text{BTAH}_{(ads)}$ + $O_{(ads)}$ reaction: $\Delta E_{\text{deproto}}$ monotonically increases (becomes more endothermic) with the $O_{(ads)}$ coverage, but the increase is only 0.12 eV at the highest coverage.
2. The $\text{BTAH}_{(ads)}$ + $OH_{(ads)}$ reaction: reaction energies become more exothermic as the $OH_{(ads)}$ coverage increases (except at 2/16 ML) such that at the highest coverage, the reaction is more exothermic by 0.15 eV compared to the low 1/16 ML coverage.
3. The $\text{ImiH}_{(ads)}$ + $O_{(ads)}$ reaction: $\Delta E_{\text{deproto}}$ is rather insensitive to the $O_{(ads)}$ coverage because all the values are within [−0.26, −0.20] eV.
4. The $\text{ImiH}_{(ads)}$ + $OH_{(ads)}$ reaction: $\Delta E_{\text{deproto}}$ decreases by about 0.1 eV (becomes more exothermic) from 1/16 to 3/16 ML and then increases.

Based on these results (Fig. 7), we can thus conclude that the deprotonation reactions are favorable at least up to the 4/16 ML coverage of $X_{(ads)}$. Furthermore, based on the observation that deprotonation reaction energies do not show a strong dependence on the $X_{(ads)}$ coverage, we can also anticipate that activation energies should not depend strongly on the $X_{(ads)}$ coverage. This reasoning is supported by a thorough study [49], which shows that dissociation reactions obey the Brønsted-Evans-Polanyi linear relation between activation (E^*) and reaction (ΔE) energies, $E^* = a + b\Delta E$. For the X–H cleavage reactions, the b factor is close to one [49], implying that ΔE and E^* vary similarly.

To conjecture what would happen at even higher $X_{(ads)}$ coverage than currently considered, it is worth observing that deprotonated molecules bond to more surface Cu atoms than intact molecules (intact ImiH and BTAH on X/Cu(111) bond to a single surface Cu atom,

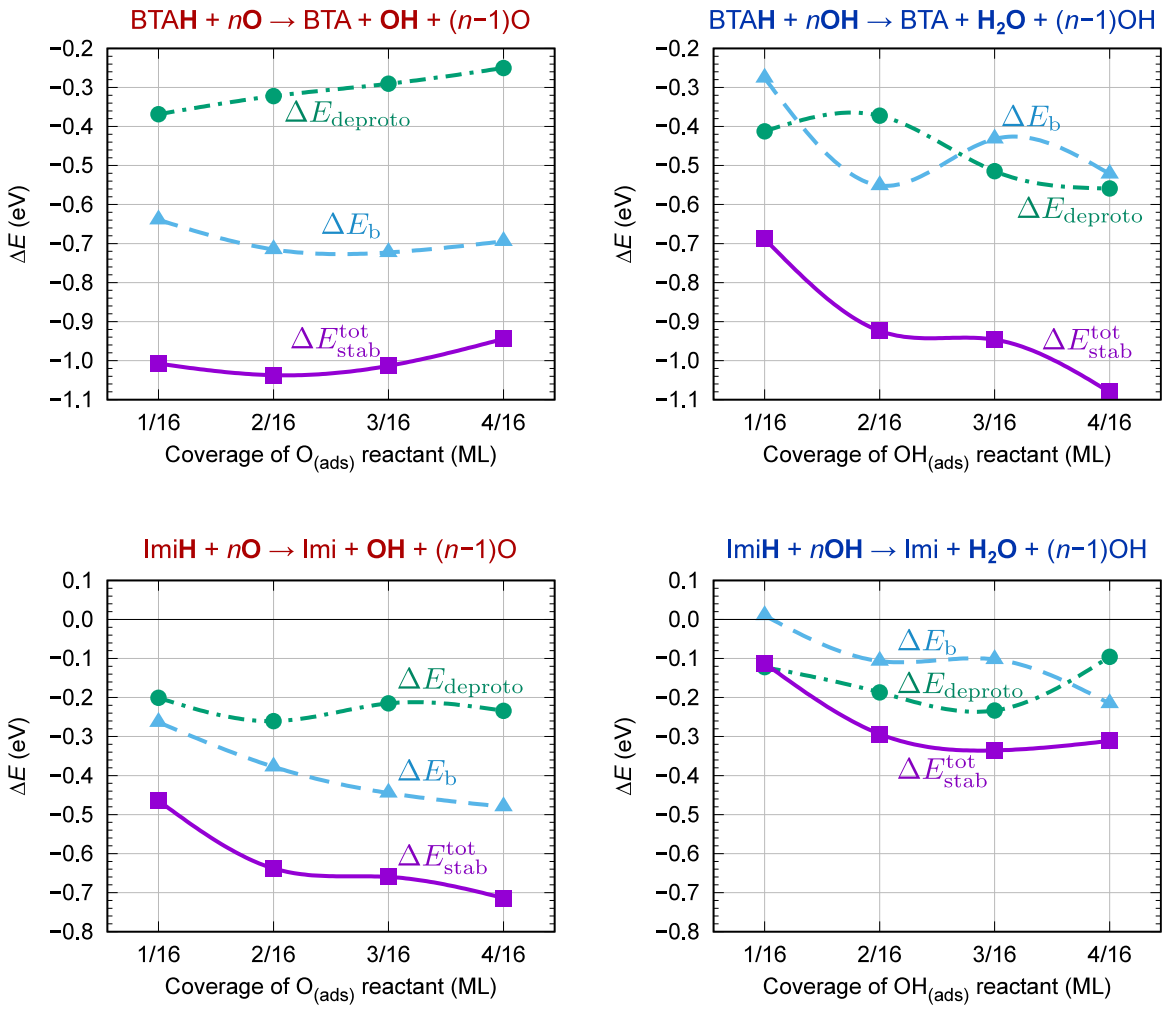

Fig. 8. Dependence of the total stabilization energy, $\Delta E^{\mathrm{tot}}_{\mathrm{stab}}$ of Eq. (11), and its ΔE_{b} and $\Delta E_{\mathrm{deproto}}$ components on the coverage of $X_{(\mathrm{ads})}$ for BTAH (top row) and ImiH (bottom row). Beware of the different energy scales for BTAH and ImiH. Curves are drawn to guide the eye. Graphs in the left and right columns correspond to reactions with $O_{(\mathrm{ads})}$ and $OH_{(\mathrm{ads})}$, respectively. Only the most stable identified structures at each coverage are considered, which correspond to solid data points in Fig. 7 (snapshots of the corresponding structures are shown in Figs. S9–S12 in the Supplementary material).

whereas deprotonated molecules bond to two or three Cu atoms). We can therefore anticipate that if the coverage of $X_{(\mathrm{ads})}$ would become so high that nearly all adsorption sites are occupied, then deprotonation could remain feasible at $X_{(\mathrm{ads})}$ vacancies (i.e., surface patches with unoccupied surface sites), as confirmed for deprotonation of triazole and tetrazole at oxygen vacancies on $Cu_2O(111)$ [42].

Let us also quantify the total stabilization of molecular adsorption induced by $X_{(\mathrm{ads})}$, $\Delta E^{\mathrm{tot}}_{\mathrm{stab}}$ of Eq. (11). $\Delta E^{\mathrm{tot}}_{\mathrm{stab}}$ is the sum of the ΔE_{b} and $\Delta E_{\mathrm{deproto}}$ contributions, corresponding to the $X_{(\mathrm{ads})}$ induced enhancement of the MolH adsorption bonding (the ΔE_{b} term) and the additional stabilization due to a deprotonation reaction ($\Delta E_{\mathrm{deproto}}$). To this end, we will analyze only the most stable cases corresponding to the solid data points in Fig. 7. The corresponding PBE+D" calculated results are shown in Fig. 8 for all four considered combinations (MolH = BTAH or ImiH; X = O or OH). It should be noted that the ΔE_{b} values were calculated for compatible MolH + nX @ Cu(111) and nX @ Cu(111) structures, where compatibility was achieved by removing the molecule from MolH + nX @ Cu(111) and relaxing the so obtained nX @ Cu(111) structure; the corresponding bare nX @ Cu(111), reactant MolH + nX @ Cu(111), and product Mol + XH + (n−1)X @ Cu(111) structures are shown in Figs. S9–S12 in the Supplementary material.

We first discuss the stabilization induced by $O_{(\mathrm{ads})}$ (left column of Fig. 8). In addition to exothermic $\Delta E_{\mathrm{deproto}}$ discussed above, the ΔE_{b} values are also exothermic. For BTAH, the total $O_{(\mathrm{ads})}$ induced stabilization, $\Delta E^{\mathrm{tot}}_{\mathrm{stab}}$, is about −1 eV for the $O_{(\mathrm{ads})}$ coverages up to 3/16 ML, whereas at 4/16 ML, the stabilization is slightly weaker, −0.94 eV. For ImiH, the total $O_{(\mathrm{ads})}$ induced stabilization is weaker than for BTAH and ranges from about −0.5 eV at 1/16 ML to about −0.7 eV at 4/16 ML.

As for the $OH_{(\mathrm{ads})}$ induced stabilization (right column of Fig. 8), ΔE_{b} tends to become more exothermic as the $OH_{(\mathrm{ads})}$ coverage increases (with some oscillation at 3/16 ML), such that at the high 4/16 ML coverage ΔE_{b} is by about 0.25 eV more exothermic than at low 1/16 ML coverage. For BTAH, the total $OH_{(\mathrm{ads})}$ induced stabilization, $\Delta E^{\mathrm{tot}}_{\mathrm{stab}}$, strengthens with coverage and reaches about −1.1 eV at 4/16 ML. For ImiH, the total $OH_{(\mathrm{ads})}$ induced stabilization is considerably weaker than for BTAH, being about −0.1 eV at low 1/6 ML and about −0.3 eV at higher coverages.

The finding that the $\Delta E^{\mathrm{tot}}_{\mathrm{stab}}$ values are considerably less exothermic for ImiH than for BTAH can be explained by observing that deprotonation of BTAH involves the cleavage of the N–H bond, whereas for ImiH the C–H bond is cleaved. The latter bond is more difficult to cleave because the corresponding activation energies are sizable (Fig. 5). In contrast, the activation energies for the cleavage of the N–H bonds are considerably smaller, i.e., vanishing for BTAH (Fig. 4) and about 0.1 eV for ImiH (Fig. 6). However, the N1–H deprotonated imidazole forms

Table 1
PBE+D" calculated adsorption energies of non-dissociative and dissociative adsorption of BTAH and ImiH on bare Cu(111), O/Cu(111), and OH/Cu(111). Calculations were performed at a molecular coverage of 1/16 ML using the (4×4)–Cu(111) supercell. Θ_X stands for the surface coverage of $O_{(ads)}$ or $OH_{(ads)}$. ΔE_b is the difference between a given non-dissociative E_{ads} on X/Cu(111) and that on bare Cu(111), whereas ΔE^{tot}_{stab} is the difference between a given dissociative E^{diss}_{ads} on X/Cu(111) and non-dissociative E_{ads} on bare Cu(111).

Surface	Θ_X (ML)	Adsorption mode	E_{ads} (eV)	ΔE_b (eV)	Adsorption mode	E^{diss}_{ads} (eV)	ΔE^{tot}_{stab} (eV)
		non-dissociative BTAH			disociative H + BTA$^{(N1)}$		
Cu(111)	0		−0.74	/		−0.92	−0.18
O/Cu(111)	1/16		−1.37	−0.64		−1.74	−1.00
	2/16		−1.45	−0.72		−1.77	−1.03
	3/16		−1.46	−0.72		−1.75	−1.01
	4/16		−1.43	−0.69		−1.68	−0.94
OH/Cu(111)	1/16		−1.01	−0.27		−1.42	−0.68
	2/16		−1.29	−0.55		−1.66	−0.92
	3/16		−1.17	−0.43		−1.68	−0.94
	4/16		−1.26	−0.52		−1.82	−1.08
		non-dissociative ImiH			disociative H + Imi$^{(C2)}$		
Cu(111)	0		−0.83	/		−0.63	+0.20
O/Cu(111)	1/16		−1.09	−0.26		−1.29	−0.46
	2/16		−1.21	−0.38		−1.47	−0.64
	3/16		−1.28	−0.45		−1.49	−0.66
	4/16		−1.31	−0.48		−1.55	−0.72
OH/Cu(111)	1/16		−0.82	+0.01		−0.94	−0.11
	2/16		−0.94	−0.11		−1.12	−0.29
	3/16		−0.93	−0.10		−1.17	−0.34
	4/16		−1.05	−0.22		−1.14	−0.31

only one N–Cu bond,[6] whereas the C2–H deprotonated imidazole forms N–Cu and C–Cu bonds and is, therefore, more stable despite its much higher activation energy.

3.5. Adsorption energies and persistence of molecules on surfaces

So far, the focus of the discussion was on the $O_{(ads)}$ and $OH_{(ads)}$ induced stabilization of molecular adsorption via the ΔE_b and $\Delta E_{deproto}$ contributions. To complete the discussion, we now discuss the adsorption energies presented in Table 1. On bare Cu(111) at molecular coverage of 1/16 ML, the PBE+D" calculated non-dissociative adsorption energies of BTAH and ImiH are −0.74 eV and −0.83 eV, respectively. It is worth commenting that the adsorption energies of azoles depend on the coverage due to long-ranged lateral intermolecular interactions, which result from sizable permanent dipole moments of azole molecules [50–52].

For BTAH, the $O_{(ads)}$ and $OH_{(ads)}$ induced ΔE^{tot}_{stab} stabilization reaches the value of about −1.0 to −1.1 eV, hence the corresponding dissociative adsorption energies are sizable, around −1.7 to −1.8 eV. Such a strong enhancement of adsorption energy has important consequences because it exponentially increases a molecular residence time on a surface. A typical residence time (τ) can be estimated from the inverted Arrhenius equation, $\tau = \nu^{-1}\exp(E_{des}/kT)$, where ν is the frequency prefactor, E_{des} is the desorption energy, and k is the Boltzmann constant. By assuming that desorption energy is given by the magnitude of adsorption energy and using the value of $\nu = 10^{16}$ s^{-1} for the frequency prefactor of desorption [53–55], a typical residence time of BTAH on Cu(111) ($E_{ads} = -0.74$ eV) and X/Cu(111) ($E^{diss}_{ads} \approx -1.7$ eV) at room temperature is estimated to 0.3 millisecond and about 200,000 years, respectively. BTAH thus quickly desorbs from bare Cu(111), whereas on O/Cu(111) and OH/Cu(111), its dissociative adsorption appears irreversible for the human perception of time.

[6] Imidazole has two N atoms on the opposite side of the molecule and can form either one strong N–Cu bond or two strained N–Cu bonds with the surface.

Table 2
Comparison between the *in-vacuo* and approximate aqueous-phase activation (E^*) and reaction ($\Delta E_{deproto}$) energies for BTAH and ImiH deprotonation on O/Cu(111) and OH/Cu(111); aqueous-phase values are written in parentheses. Calculations were performed at a molecular coverage of 1/16 ML using the (4×4)–X/Cu(111) supercell. Both N1–H and C2–H bond cleavages are considered for imidazole.

Reaction	E^* (eV) vacuum (aqueous)	$\Delta E_{deproto}$ (eV) vacuum (aqueous)
$BTAH_{(ads)} + O_{(ads)} \rightarrow BTA_{(ads)} + OH_{(ads)}$	0.02 (0.01)	−0.37 (−0.28)
$BTAH_{(ads)} + OH_{(ads)} \rightarrow BTA_{(ads)} + H_2O_{(ads)}$	0.01 (0.01)	−0.42 (−0.38)
$ImiH_{(ads)} + O_{(ads)} \rightarrow Imi_{(ads)} + OH_{(ads)}$		
N1–H bond cleavage	0.11 (0.14)	+0.06 (+0.23)
C2–H bond cleavage	0.63 (0.73)	−0.20 (+0.04)
$ImiH_{(ads)} + OH_{(ads)} \rightarrow Imi_{(ads)} + H_2O_{(ads)}$		
N1–H bond cleavage	0.10 (0.08)	−0.03 (+0.09)
C2–H bond cleavage	0.89 (0.88)	−0.12 (+0.02)

For ImiH, the strongest dissociative adsorption energies are about −1.5 and −1.2 eV on O/Cu(111) and OH/Cu(111), respectively. But for ImiH, the activation barriers for the C2–H bond cleavage are sizable on X/Cu(111), from 0.63 to 0.89 eV (Fig. 5). The analysis of the adsorption and activation energies reveals that adsorption energies of ImiH on O/Cu(111) are strong enough to make deprotonation kinetically preferred over desorption. In contrast, on OH/Cu(111), it is usually the opposite.[7] For this reason, the analysis of molecular residence times for both non-dissociative and dissociative adsorption is relevant for ImiH. At room temperature, a typical residence time of non-dissociatively adsorbed ImiH on Cu(111) is about 10 milliseconds. On O/Cu(111), it is about 10 days (for the strongest calculated E_{ads} of −1.3 eV), and on OH/Cu(111), it is about 1 minute (for the strongest E_{ads} of −1.05 eV). For dissociative adsorption of ImiH on O/Cu(111), the estimated typical residence times at room temperature range from about 10 days (for the weakest E^{diss}_{ads} of −1.3 eV) to about 500 years (for the strongest E^{diss}_{ads} of −1.55 eV).

It should be noted that the above surface residence times for deprotonated molecules were estimated by assuming a recombinative two-step desorption. The first step in this two-step desorption is protonation of $Mol_{(ads)}$ and the second step is desorption of MolH. For both steps, a frequency prefactor of 10^{16} s^{-1} was assumed.

3.6. Effect of aqueous solvent on adsorption and deprotonation

All the calculations presented above were performed at the solid/vacuum interface, although the solid/water interface is relevant in the context of corrosion. For this reason, we also tried to estimate the effect of the aqueous solvent on adsorption, activation, and reaction energies using the implicit soft-sphere-continuum-solvation method [36] as implemented in the `Environ` plugin [37] for Quantum ESPRESSO.

[7] Note that the pre-exponential factors ν are 1 to 3 orders of magnitude higher for desorption than dissociation; we assumed the values of $\nu = 10^{16}$ and 10^{13} s^{-1} for desorption and deprotonation, respectively (note that with this assumption, a possible proton tunneling during deprotonation is neglected). A difference of three orders of magnitude in ν corresponds to the following difference in activation energy (ΔE^*) between the two processes: $\Delta E^* = 3kT\ln 10$, which equals 0.18 eV at room temperature. Non-dissociative adsorption energies of ImiH on O/Cu(111) range from −1.1 to −1.3 eV, whereas deprotonation activation energies range from 0.6 to 0.9 eV. Deprotonation is thus kinetically preferred even for the "worst" case combination of the two energies. The situation is different for OH/Cu(111), where non-dissociative adsorption energies of ImiH range from −0.8 to −1.1 eV and deprotonation activation energy is 0.9 eV. Hence, in this case, deprotonation is usually kinetically inferior to desorption.

Table 3
Average adsorption energies of BTAH and ImiH on OH/Cu(111), O/Cu(111), Cu(111) as obtained with *in-vacuo* and approximate aqueous-phase calculations; aqueous-phase values are written in parentheses. Differences between aqueous-phase and *in-vacuo* average adsorption energies are also reported, i.e., $\Delta\langle E_{\mathrm{ads}}\rangle = \langle E_{\mathrm{ads}}(\mathrm{aqueous})\rangle - \langle E_{\mathrm{ads}}(\mathrm{vacuum})\rangle$ and $\Delta\langle E^{\mathrm{diss}}_{\mathrm{ads}}\rangle$ is defined likewise. Average adsorption energies are calculated as $\langle E_{\mathrm{ad}}\rangle = \frac{1}{4}(E^{1/16}_{\mathrm{ad}} + E^{2/16}_{\mathrm{ad}} + E^{3/16}_{\mathrm{ad}} + E^{4/16}_{\mathrm{ad}})$, where E_{ad} stands for either E_{ads} or $E^{\mathrm{diss}}_{\mathrm{ads}}$ and the superscript $n/16$ indicates that E_{ad} corresponds to the $X_{(\mathrm{ads})}$ coverage of $n/16$ ML. For bare Cu(111), the reported values correspond to adsorption energies at a molecular coverage of 1/16 ML.

Surface	Adsorption mode	$\langle E_{\mathrm{ads}}\rangle$ (eV) vacuum	(aqueous)	$\Delta\langle E_{\mathrm{ads}}\rangle$ (eV)	Adsorption mode	$\langle E^{\mathrm{diss}}_{\mathrm{ads}}\rangle$ (eV) vacuum	(aqueous)	$\Delta\langle E^{\mathrm{diss}}_{\mathrm{ads}}\rangle$ (eV)
	non-dissociative BTAH				disociative H + $\mathrm{BTA}^{(\mathrm{N1})}$			
Cu(111)		−0.74[a]	(−0.38[a])	0.36		−0.92[a]	(−0.61[a])	0.31
O/Cu(111)		−1.43	(−0.85)	0.58		−1.74	(−1.06)	0.68
OH/Cu(111)		−1.18	(−0.78)	0.40		−1.64	(−1.20)	0.44
	non-dissociative ImiH				disociative H + $\mathrm{Imi}^{(\mathrm{C2})}$			
Cu(111)		−0.83[a]	(−0.53[a])	0.30		−0.63[a]	(−0.13[a])	0.50
O/Cu(111)		−1.22	(−0.70)	0.52		−1.45	(−0.65)	0.80
OH/Cu(111)		−0.94	(−0.65)	0.29		−1.09	(−0.67)	0.42

[a]Corresponds to the adsorption energy at a molecular coverage of 1/16 ML.

Due to convergence problems, we could only perform single-point SCF calculations of the structures relaxed in a vacuum. Hence, the corresponding results should be taken cautiously and serve only as an indication.

As for deprotonation reactions, a comparison with the *in-vacuo* results (Table 2) reveals that the presence of the implicit aqueous solvent only weakly affects the activation barriers. The most significant difference occurs for the $\mathrm{ImiH}_{(\mathrm{ads})} + \mathrm{O}_{(\mathrm{ads})} \rightarrow \mathrm{Imi}_{(\mathrm{ads})} + \mathrm{OH}_{(\mathrm{ads})}$ reaction, where the activation energy is 0.1 eV higher than in a vacuum. In contrast, the reaction energies are affected more significantly, and the current results indicate that the presence of an aqueous solvent makes deprotonations of adsorbed molecules less exothermic by 0.1 to 0.2 eV. Consequently, deprotonation of imidazole becomes weakly endothermic at the solid/water interface, but the imidazole's C2–H bond cleavage remains thermodynamically superior to the N1–H bond cleavage.

The aqueous solvent also diminishes the adsorption energy magnitudes, which is reasonable because, during adsorption, both a molecule and a surface around the adsorption site must partially desolvate. This trend is evident from Table S1 in the Supplementary material, which is an extended version of Table 1 with both *in-vacuo* and aqueous-phase adsorption energies reported. To facilitate the comprehension of these extensive data, the values were averaged over the $X_{(\mathrm{ads})}$ coverages, and the corresponding average adsorption energies are reported in Table 3. This table reveals that the aqueous solvent significantly diminishes the adsorption energy magnitudes, from 0.3 to 0.6 eV for non-dissociative adsorption and from 0.3 to 0.8 eV for dissociative adsorption. Consequently, the strongest calculated adsorption energy at the solid/water interface is about −1.2 eV for BTAH and about −0.7 eV for ImiH.

4. Conclusions

With DFT calculations, we scrutinized how chemisorbed O and OH affect the adsorption of benzotriazole and imidazole on Cu(111). The focus was on deprotonation reactions promoted by $\mathrm{O}_{(\mathrm{ads})}$ and $\mathrm{OH}_{(\mathrm{ads})}$, where the role of their coverage was also addressed.

The $X_{(\mathrm{ads})}$ induced stabilization of molecular adsorption is twofold: (i) $X_{(\mathrm{ads})}$ can enhance adsorption bonding of intact azole molecules (the ΔE_{b} contribution); for both imidazole and benzotriazole, $\mathrm{O}_{(\mathrm{ads})}$ displays more stabilizing ΔE_{b} than $\mathrm{OH}_{(\mathrm{ads})}$. (ii) The adsorbed molecules are further stabilized by deprotonation (the $\Delta E_{\mathrm{deproto}}$ contribution) that involves a proton shift from the molecule to the nearby $\mathrm{O}_{(\mathrm{ads})}$ or $\mathrm{OH}_{(\mathrm{ads})}$. Deprotonation of adsorbed benzotriazole proceeds via the N–H bond cleavage with a marginally small activation barrier of the order of 0.01 eV. The N–H bond cleavage with an activation barrier of about 0.1 eV is also kinetically feasible for imidazole, although the C–H bond cleavage is thermodynamically preferred (but shows considerably higher activation energies, from 0.6 to 0.9 eV). The thermodynamic inferiority of imidazole's N–H cleavage can be attributed to its molecular structure with the two N atoms on opposite sides of the molecule.

Current findings can be generalized to other azole molecules by conjecturing that, on copper surfaces, deprotonations involving the heteroatom–H bond cleavage display much smaller activation barriers than deprotonations involving the C–H bond cleavage. Indeed, small (or even vanishing) activation energies were also observed for the N–H bond cleavage of triazole, tetrazole, and mercaptobenzimidazole on oxidized copper surfaces [42,56] and for the S–H bond cleavage of mercaptobenzimidazole on Cu(111) [57,58].

The $X_{(\mathrm{ads})}$ induced total stabilization ($\Delta E_{\mathrm{b}} + \Delta E_{\mathrm{deproto}}$) is stronger for BTAH than for ImiH. It reaches the magnitude of about 1 eV for benzotriazole on X/Cu(111) and about 0.7 eV and 0.3 eV for imidazole on O/Cu(111) and OH/Cu(111), respectively. The increased energy stability of adsorbed molecules exponentially increases their persistence on surfaces. This observation is relevant in the context of corrosion inhibition because inhibitor molecules must persist on the surface to inhibit corrosion. For BTAH, dissociative adsorption energies reach the value of about −1.8 eV on O/Cu(111) and OH/Cu(111), which is a value strong enough to make the adsorption of BTAH irreversible (within the human time-frame) at room temperature.

A critique of the presented results is that calculations were performed at the solid/vacuum interface, while the solid/water interface is relevant in the context of corrosion. Hence, by using an implicit solvent method, we also roughly estimated the effect of water solvent on molecular adsorption and subsequent deprotonation. These calculations revealed that the aqueous solvent weakly affects the activation barriers for the deprotonation of adsorbed molecules (typically a few tens of meV), whereas the deprotonation reaction energies become less exothermic by up to about 0.2 eV. In contrast, adsorption energy magnitudes reduce considerably in the aqueous phase, from 0.3 to 0.8 eV. Despite this significant reduction, the adsorption energy still appears sufficiently strong for BTAH to persist on the surface at room temperature.

Declaration of competing interest

The authors declare that they have no known competing financial interests or personal relationships that could have appeared to influence the work reported in this paper.

Data availability

Data will be made available on request.

Acknowledgments

This work is a part of the M-Era.Net project entitled "Coin Desc: Corrosion inhibition and dealloying descriptors". The financial support of the project by MESS (Ministry of Education, Science and Sport of Republic of Slovenia, Grant No. C3330-17-500074) is acknowledged. This work has been also supported by the Slovenian Research Agency (Grant Nos. P2-0393 and PR-08976).

Appendix A. Supplementary data

Supplementary material related to this article can be found online at https://doi.org/10.1016/j.corsci.2022.110680.

References

[1] J. O'M. Bockris, A.K.N. Reddy, Modern Electrochemistry, second ed., vol. 2B, Kluwer Academic/Plenum Publishers, New York, 2000.
[2] A. Kokalj, Molecular modeling of organic corrosion inhibitors: Calculations, pitfalls, and conceptualization of molecule–surface bonding, Corros. Sci. 193 (2021) 109650, http://dx.doi.org/10.1016/j.corsci.2021.109650.
[3] I.B. Obot, D.D. Macdonald, Z.M. Gasem, Density functional theory (DFT) as a powerful tool for designing new organic corrosion inhibitors. Part 1: An overview, Corros. Sci. 99 (2015) 1–30, http://dx.doi.org/10.1016/j.corsci.2015.01.037, URL http://www.sciencedirect.com/science/article/pii/S0010938X15000487.
[4] M. Dlouhy, A. Kokalj, How adsorbed H, O, OH, and Cl affect plain adsorption of imidazole on copper, Corros. Sci. 205 (2022) 110443, http://dx.doi.org/10.1016/j.corsci.2022.110443.
[5] Y.I. Kuznetsov, L.P. Kazansky, Physicochemical aspects of metal protection by azoles as corrosion inhibitors, Russ. Chem. Rev. 77 (2008) 219–232, http://dx.doi.org/10.1070/rc2008v077n03abeh003753.
[6] M. Finšgar, I. Milošev, Inhibition of copper corrosion by 1,2,3-benzotriazole: A review, Corros. Sci. 52 (9) (2010) 2737–2749, http://dx.doi.org/10.1016/j.corsci.2010.05.002.
[7] Y. Jiang, J.B. Adams, First principle calculations of benzotriazole adsorption onto clean Cu(111), Surf. Sci. 529 (2003) 428–442, http://dx.doi.org/10.1016/S0039-6028(03)00277-2, URL https://www.sciencedirect.com/science/article/pii/S0039602803002772.
[8] A. Kokalj, N. Kovačević, S. Peljhan, M. Finšgar, A. Lesar, I. Milošev, Triazole, benzotriazole, and naphthotriazole as copper corrosion inhibitors: I. Molecular electronic and adsorption properties, ChemPhysChem 12 (18) (2011) 3547–3555, http://dx.doi.org/10.1002/cphc.201100537, URL https://chemistry-europe.onlinelibrary.wiley.com/doi/10.1002/cphc.201100537.
[9] A. Kokalj, S. Peljhan, M. Finšgar, I. Milošev, What determines the inhibition effectiveness of ATA, BTAH, and BTAOH corrosion inhibitors on copper? J. Am. Chem. Soc. 132 (46) (2010) 16657–16668, http://dx.doi.org/10.1021/ja107704y, URL http://pubs.acs.org/doi/abs/10.1021/ja107704y.
[10] X. Chen, H. Häkkinen, Divide and protect: Passivating Cu(111) by Cu-(benzotriazole)$_2$, J. Phys. Chem. C 116 (42) (2012) 22346–22349, http://dx.doi.org/10.1021/jp3055894, URL http://pubs.acs.org/doi/abs/10.1021/jp3055894.
[11] S. Peljhan, J. Koller, A. Kokalj, The effect of surface geometry of copper on adsorption of benzotriazole and Cl. Part I, J. Phys. Chem. C 118 (2) (2014) 933–943, http://dx.doi.org/10.1021/jp409717e, URL http://pubs.acs.org/doi/abs/10.1021/jp409717e.
[12] A. Kokalj, S. Peljhan, Density functional theory study of adsorption of benzotriazole on Cu_2O surfaces, J. Phys. Chem. C 119 (2015) 11625–11635, http://dx.doi.org/10.1021/acs.jpcc.5b01677.
[13] F. Grillo, D.W. Tee, S.M. Francis, H.A. Früchtl, N.V. Richardson, Passivation of copper: Benzotriazole films on Cu(111), J. Phys. Chem. C 118 (16) (2014) 8667–8675, http://dx.doi.org/10.1021/jp411482e, URL http://pubs.acs.org/doi/abs/10.1021/jp411482e.
[14] C. Gattinoni, A. Michaelides, Understanding corrosion inhibition with van der Waals DFT methods: the case of benzotriazole, Faraday Discuss. 180 (2015) 439–458, http://dx.doi.org/10.1039/C4FD00273C.
[15] C. Gattinoni, P. Tsaousis, C. Euaruksakul, R. Price, D.A. Duncan, T. Pascal, D. Prendergast, G. Held, A. Michaelides, Adsorption behavior of organic molecules: A study of benzotriazole on Cu(111) with spectroscopic and theoretical methods, Langmuir 35 (4) (2019) 882–893, http://dx.doi.org/10.1021/acs.langmuir.8b03528.
[16] M. Turano, M. Walker, F. Grillo, C. Gattinoni, J. Edmondson, O. Adesida, G. Hunt, P.M. Kirkman, N.V. Richardson, C.J. Baddeley, A. Michaelides, G. Costantini, Understanding the interaction of organic corrosion inhibitors with copper at the molecular scale: Benzotriazole on Cu(110), Appl. Surf. Sci. 570 (2021) 151206, http://dx.doi.org/10.1016/j.apsusc.2021.151206.
[17] N. Kovačević, A. Kokalj, The relation between adsorption bonding and corrosion inhibition of azole molecules on copper, Corros. Sci. 73 (2013) 7–17, http://dx.doi.org/10.1016/j.corsci.2013.03.016, URL http://www.sciencedirect.com/science/article/pii/S0010938X13000954.
[18] S. Sun, Y. Geng, L. Tian, S. Chen, Y. Yan, S. Hu, Density functional theory study of imidazole, benzimidazole and 2-mercaptobenzimidazole adsorption onto clean Cu(111) surface, Corros. Sci. 63 (2012) 140–147, http://dx.doi.org/10.1016/j.corsci.2012.05.024, URL http://www.sciencedirect.com/science/article/pii/S0010938X12002703.
[19] H. Wang, Y. Hao, S. Chen, M. Cheng, C. Li, S. Sun, S. Hu, DFT study of imidazoles adsorption on the grain boundary of Cu(100) surface, Corros. Sci. 137 (2018) 33–42, http://dx.doi.org/10.1016/j.corsci.2018.03.009, URL http://www.sciencedirect.com/science/article/pii/S0010938X17312039.
[20] D. Kumar, V. Jain, B. Rai, Imidazole derivatives as corrosion inhibitors for copper: A DFT and reactive force field study, Corros. Sci. 171 (2020) 108724, http://dx.doi.org/10.1016/j.corsci.2020.108724.
[21] A. Kokalj, S. Peljhan, J. Koller, The effect of surface geometry of copper on dehydrogenation of benzotriazole. Part II, J. Phys. Chem. C 118 (2) (2014) 944–954, http://dx.doi.org/10.1021/jp409719c, URL http://pubs.acs.org/doi/abs/10.1021/jp409719c.
[22] A. Kokalj, D. Gustinčič, M. Poberžnik, M. Lozinšek, New insights into adsorption bonding of imidazole: A viable C2–H bond cleavage on copper surfaces, Appl. Surf. Sci. 479 (2019) 463–468, http://dx.doi.org/10.1016/j.apsusc.2018.12.246, URL http://www.sciencedirect.com/science/article/pii/S0169433218335943.
[23] P. Giannozzi, S. Baroni, N. Bonini, M. Calandra, R. Car, C. Cavazzoni, D. Ceresoli, G.L. Chiarotti, M. Cococcioni, I. Dabo, A. Dal Corso, S. de Gironcoli, S. Fabris, G. Fratesi, R. Gebauer, U. Gerstmann, C. Gougoussis, A. Kokalj, M. Lazzeri, L. Martin-Samos, N. Marzari, F. Mauri, R. Mazzarello, S. Paolini, A. Pasquarello, L. Paulatto, C. Sbraccia, S. Scandolo, G. Sclauzero, A.P. Seitsonen, A. Smogunov, P. Umari, R.M. Wentzcovitch, Quantum ESPRESSO: a modular and open-source software project for quantum simulations of materials, J. Phys: Condens. Matter 21 (39) (2009) 395502, http://dx.doi.org/10.1088/0953-8984/21/39/395502, URL https://iopscience.iop.org/article/10.1088/0953-8984/21/39/395502.
[24] P. Giannozzi, O. Andreussi, T. Brumme, O. Bunau, M.B. Nardelli, M. Calandra, R. Car, C. Cavazzoni, D. Ceresoli, M. Cococcioni, N. Colonna, I. Carnimeo, A.D. Corso, S. de Gironcoli, P. Delugas, R. DiStasio, A. Ferretti, A. Floris, G. Fratesi, G. Fugallo, R. Gebauer, U. Gerstmann, F. Giustino, T. Gorni, J. Jia, M. Kawamura, H.-Y. Ko, A. Kokalj, E. Küçükbenli, M. Lazzeri, M. Marsili, N. Marzari, F. Mauri, N.L. Nguyen, H.-V. Nguyen, A.O. de-la Roza, L. Paulatto, S. Poncé, D. Rocca, R. Sabatini, B. Santra, M. Schlipf, A.P. Seitsonen, A. Smogunov, I. Timrov, T. Thonhauser, P. Umari, N. Vast, X. Wu, S. Baroni, Advanced capabilities for materials modelling with Quantum ESPRESSO, J. Phys: Condens. Matter 29 (2017) 465901, http://dx.doi.org/10.1088/1361-648X/aa8f79, URL http://iopscience.iop.org/article/10.1088/1361-648X/aa8f79.
[25] D. Gustinčič, A. Kokalj, A DFT study of adsorption of imidazole, triazole, and tetrazole on oxidized copper surfaces: $Cu_2O(111)$ and $Cu_2O(111)$-w/o-Cu^{CUS}, Phys. Chem. Chem. Phys. 17 (2015) 28602–28615, http://dx.doi.org/10.1039/C5CP03647J.
[26] J.P. Perdew, K. Burke, M. Ernzerhof, Generalized gradient approximation made simple, Phys. Rev. Lett. 77 (18) (1996) 3865–3868, http://dx.doi.org/10.1103/PhysRevLett.77.3865, URL https://journals.aps.org/prl/abstract/10.1103/PhysRevLett.77.3865.
[27] S. Grimme, Semiempirical GGA-type density functional constructed with a long-range dispersion correction, J. Phys: Condens. Matter 27 (15) (2006) 1787–1799, http://dx.doi.org/10.1002/jcc.20495, URL https://onlinelibrary.wiley.com/doi/10.1002/jcc.20495.
[28] D. Vanderbilt, Soft self-consistent pseudopotentials in a generalized eigenvalue formalism, Phys. Rev. B 41 (1990) 7892–7895, http://dx.doi.org/10.1103/PhysRevB.41.7892, URL https://link.aps.org/doi/10.1103/PhysRevB.41.7892.
[29] Ultrasoft pseudopotentials for H, C, N, O, Cl, and Cu atoms were taken from the quantum espresso pseudopotential download page at (files: `H.pbe-rrkjus.UPF`, `C.pbe-rrkjus.UPF`, `N.pbe-rrkjus.UPF`, `O.pbe-rrkjus.UPF`, `Cl.pbe-n-van.UPF`, and `Cu.pbe-d-rrkjus.UPF`)., 2021, http://www.quantum-espresso.org/pseudopotentials.
[30] A. Kokalj, PWTK: PWscf ToolKit, 2021, Code available from http://pwtk.ijs.si/.
[31] L. Bengtsson, Dipole correction for surface supercell calculations, Phys. Rev. B 59 (19) (1999) 12301–12304, http://dx.doi.org/10.1103/PhysRevB.59.12301.
[32] H.J. Monkhorst, J.D. Pack, Special points for Brillouin-zone integrations, Phys. Rev. B 13 (12) (1976) 5188–5192, http://dx.doi.org/10.1103/PhysRevB.13.5188, URL https://journals.aps.org/prb/abstract/10.1103/PhysRevB.13.5188.
[33] M. Methfessel, A.T. Paxton, High-precision sampling for Brillouin-zone integration in metals, Phys. Rev. B 40 (1989) 3616–3621, http://dx.doi.org/10.1103/PhysRevB.40.3616, URL http://link.aps.org/doi/10.1103/PhysRevB.40.3616.
[34] G. Henkelman, H. Jónsson, Improved tangent estimate in the nudged elastic band method for finding minimum energy paths and saddle points, J. Chem. Phys. 113 (22) (2000) 9978–9985, http://dx.doi.org/10.1063/1.1323224, URL https://aip.scitation.org/doi/abs/10.1063/1.1323224.
[35] G. Henkelman, B.P. Uberuaga, H. Jónsson, A climbing image nudged elastic band method for finding saddle points and minimum energy paths, J. Chem. Phys. 113 (22) (2000) 9901–9904, http://dx.doi.org/10.1063/1.1329672, URL https://aip.scitation.org/doi/abs/10.1063/1.1329672.

[36] G. Fisicaro, L. Genovese, O. Andreussi, S. Mandal, N.N. Nair, N. Marzari, S. Goedecker, Soft-sphere continuum solvation in electronic-structure calculations, J. Chem. Theory Comput. 13 (8) (2017) 3829–3845, http://dx.doi.org/10.1021/acs.jctc.7b00375, URL https://pubs.acs.org/doi/10.1021/acs.jctc.7b00375.

[37] O. Andreussi, I. Dabo, N. Marzari, Revised self-consistent continuum solvation in electronic-structure calculations, J. Phys. Chem. 136 (6) (2012) 064102, http://dx.doi.org/10.1063/1.3676407.

[38] A. Kokalj, XCrySDen—a new program for displaying crystalline structures and electron densities, J. Mol. Graph. Model. 17 (1999) 176–179, http://dx.doi.org/10.1016/S1093-3263(99)00028-5.

[39] T. Williams, C. Kelley, et al., Gnuplot 5.4, 2020, http://www.gnuplot.info/.

[40] Inkscape Project, Inkscape, 2021, URL https://inkscape.org.

[41] A. Kokalj, Ab initio modeling of the bonding of benzotriazole corrosion inhibitor to reduced and oxidized copper surfaces, Faraday Discuss. 180 (2015) 415–438, http://dx.doi.org/10.1039/C4FD00257A.

[42] D. Gustinčič, A. Kokalj, DFT study of azole corrosion inhibitors on Cu_2O model of oxidized copper surfaces: I. Molecule–surface and Cl–surface bonding, Metals 8 (5) (2018) 310, http://dx.doi.org/10.3390/met8050310, URL http://www.mdpi.com/2075-4701/8/5/310.

[43] N. Kovačević, I. Milošev, A. Kokalj, How relevant is the adsorption bonding of imidazoles and triazoles for their corrosion inhibition of copper? Corros. Sci. 124 (2017) 25–34, http://dx.doi.org/10.1016/j.corsci.2017.04.021, URL http://www.sciencedirect.com/science/article/pii/S0010938X16307715.

[44] N. Kovačević, A. Kokalj, Chemistry of the interaction between azole type corrosion inhibitor molecules and metal surfaces, Mater. Chem. Phys. 137 (1) (2012) 331–339, http://dx.doi.org/10.1016/j.matchemphys.2012.09.030, URL http://www.sciencedirect.com/science/article/pii/S0254058412008176.

[45] A. Kokalj, Formation and structure of inhibitive molecular film of imidazole on iron surface, Corros. Sci. 68 (2013) 195–203, http://dx.doi.org/10.1016/j.corsci.2012.11.015, URL http://www.sciencedirect.com/science/article/pii/S0010938X12005574.

[46] L. Gašparič, M. Poberžnik, A. Kokalj, DFT study of hydrogen bonding between metal hydroxides and organic molecules containing N, O, S, and P heteroatoms: clusters vs. surfaces, Chem. Phys. 559 (2022) 111539, http://dx.doi.org/10.1016/j.chemphys.2022.111539.

[47] J.-Y. Jhuang, S.-H. Lee, S.-W. Chen, Y.-H. Chen, Y.-J. Chen, J.-L. Lin, C.-H. Wang, Y.-W. Yang, Adsorption and reaction pathways of 1H-pyrazole on Cu(100) and O/Cu(100), J. Phys. Chem. C 122 (11) (2018) 6195–6208, http://dx.doi.org/10.1021/acs.jpcc.8b00042.

[48] S.-W. Chen, Y.-J. Chen, Y.-H. Chen, G.-J. Chen, S.-H. Chan, J.-L. Lin, Adsorption and reaction pathways of 1H-1,2,3-triazole on Cu(100) and O/Cu(100), J. Phys. Chem. C 122 (48) (2018) 27412–27424, http://dx.doi.org/10.1021/acs.jpcc.8b08007.

[49] A. Michaelides, Z.-P. Liu, C.J. Zhang, A. Alavi, D.A. King, P. Hu, Identification of general linear relationships between activation energies and enthalpy changes for dissociation reactions at surfaces, J. Am. Chem. Soc. 125 (13) (2003) 3704–3705, http://dx.doi.org/10.1021/ja027366r, URL http://pubs.acs.org/doi/abs/10.1021/ja027366r.

[50] A. Kokalj, Electrostatic model for treating long-range lateral interactions between polar molecules adsorbed on metal surfaces, Phys. Rev. B 84 (4) (2011) 045418, http://dx.doi.org/10.1103/PhysRevB.84.045418, URL https://journals.aps.org/prb/abstract/10.1103/PhysRevB.84.045418.

[51] N. Kovačević, A. Kokalj, DFT study of interaction of azoles with Cu(111) and Al(111) surfaces: Role of azole nitrogen atoms and dipole–dipole interactions, J. Phys. Chem. C 115 (49) (2011) 24189–24197, http://dx.doi.org/10.1021/jp207076w, URL http://pubs.acs.org/doi/abs/10.1021/jp207076w.

[52] S. Peljhan, A. Kokalj, DFT study of gas-phase adsorption of benzotriazole on Cu(111), Cu(100), Cu(110), and low coordinated defects thereon, Phys. Chem. Chem. Phys. 13 (2011) 20408–20417, http://dx.doi.org/10.1039/C1CP21873E.

[53] C.T. Campbell, Y.-K. Sun, W. Weinberg, Trends in preexponential factors and activation energies in dehydrogenation and dissociation of adsorbed species, Chem. Phys. Lett. 179 (1991) 53–57, http://dx.doi.org/10.1016/0009-2614(91)90290-P, URL http://www.sciencedirect.com/science/article/pii/000926149190290P.

[54] V.P. Zhdanov, J. Pavlíeckcček, Z. Knor, Preexponential factors for elementary surface processes, Catal. Rev.: Sci. Eng. 30 (4) (1988) 501–517, http://dx.doi.org/10.1080/01614948808071752.

[55] V. Zhdanov, Arrhenius parameters for rate processes on solid surfaces, Surf. Sci. Rep. 12 (5) (1991) 185–242, http://dx.doi.org/10.1016/0167-5729(91)90011-L.

[56] F. Chiter, D. Costa, V. Maurice, P. Marcus, Atomic scale insight into corrosion inhibition: DFT study of 2-mercaptobenzimidazole on locally de-passivated copper surfaces, J. Electrochem. Soc. 168 (12) (2021) 121507, http://dx.doi.org/10.1149/1945-7111/ac405c.

[57] N. Kovačević, I. Milošev, A. Kokalj, The roles of mercapto, benzene, and methyl groups in the corrosion inhibition of imidazoles on copper: II. Inhibitor–copper bonding, Corros. Sci. 98 (2015) 457–470, http://dx.doi.org/10.1016/j.corsci.2015.05.041, URL http://www.sciencedirect.com/science/article/pii/S0010938X1500236X.

[58] Z. Zhou, Y. Zhou, Y. Huang, Q. Zhu, Y. Tang, Adsorption and dissociation of 2-mercaptobenzothiazole on Cu (1 1 1): A DFT study, Surf. Sci. 720 (2022) 122054, http://dx.doi.org/10.1016/j.susc.2022.122054.